

Fano resonances in tilted Weyl semimetals in an oscillating quantum well

Souvik Das^{♣,1}, Arnab Maity^{♣,1}, Rajib Sarkar^{♣,1}, Anirudha Menon,² Tanay Nag,^{3,4} and Banasri Basu⁵

¹*Indian Institute of Science Education and Research Kolkata, India*

²*School of Physical Sciences, Indian Association for the Cultivation of Sciences, Kolkata, India*

³*Department of Physics, BITS Pilani-Hyderabad Campus, Telangana 500078, India**

⁴*Department of Physics and Astronomy, Uppsala University, Box 516, 75120 Uppsala, Sweden*

⁵*Physics and Mathematics Unit & Interdisciplinary Statistical Research Unit, Indian Statistical Institute, Kolkata, India[†]*

(Dated: July 8, 2024)

Considering the low-energy model of tilted Weyl semimetal, we study the electronic transmission through a periodically driven quantum well, oriented in the transverse direction with respect to the tilt. We adopt the formalism of Floquet scattering theory and investigate the emergence of Fano resonances as an outcome of matching between the Floquet sidebands and quasi-bound states. The Fano resonance energy changes linearly with the tilt strength suggesting the fact that tilt-mediated part of quasi-bound state energies depends on the above factor. Given a value of momentum parallel (perpendicular) to the tilt, we find that the energy gap between two Fano resonances, appearing for two adjacent values of transverse (collinear) momentum with respect to the tilt direction, is insensitive (sensitive) to the change in the tilt strength. Such a coupled (decoupled) behavior of tilt strength and the collinear (transverse) momentum can be understood from the tilt-mediated and normal parts of the quasi-bound state energies inside the potential well. We vary the other tilt parameters and chirality of the Weyl points to conclusively verify the exact form of the tilt-mediated part of the quasi-bound state energy that is the same as the tilt term in the static dispersion. The tilt orientation can significantly alter the transport in terms of evolution of Fano resonance energy with tilt momentum. We analytically find the explicit form of the bound state energy that further supports all our numerical findings. Our work paves the way to probe the tilt-mediated part of quasi-bound state energy to understand the complex interplay between the tilt and Fano resonance.

I. INTRODUCTION

Weyl semimetals (WSMs) have been the topic of extended research in condensed matter physics over the past decade [1–6], with the proposal for and discovery of the Weyl fermion. This led to a plethora of theoretical as well as experimental studies focussing on the features, characteristics, and transport properties of such materials [7]. The minimal model of a time reversal symmetry broken WSM consists of two Weyl points which act as a source and sink for Berry curvature in momentum space. These points are usually observed near the Fermi surface where the lightcone-like dispersion of the WSM meets [1–4, 8–10]. The first proposed WSMs are now defined in the literature as the type-I WSM, which have a conical dispersion in momentum space. The addition of a Lorentz symmetry violating tilt term to the WSM Hamiltonian gives rise to a new type of WSM called the type-II WSM [11–13]. The type-II phase arises when the value of tilt generally exceeds the Fermi velocity, and this phase has some features which are distinct from the type-I phase including an extended Fermi surface. WSMs, irrespective of their type, typically exhibit a large variety of exotic properties like negative magneto-resistance [14], universal quantum Hall signatures [3, 15–18], and the chiral magnetic effect [15], all of which are some way or the other consequences of the chiral anomaly. Importantly,

the transport properties of type-II WSMs are starkly different from those of the type-I phase [19–22]. This can be ascribed to marked differences in the density of states at the Fermi level [11]. To add more, type-II WSMs possess novel quantum oscillations due to momentum space Klein tunneling [23], and a modified anomalous Hall conductivity [24]. Tilting of the Weyl cones also affects the Fano factor as described in [25]. Therefore, one can infer that the tilt-mediated transport phenomena have attracted a lot of attention in recent years.

The study of periodically driven systems has always been of great interest to physicists because of the potential to alter material behavior [26–37] and obtain phenomena which may be controlled in a laboratory environment. Periodic driving is best described by employing the Floquet formalism [38–40], which is the temporal analog of Bloch’s theorem in frequency space. The technique utilizes the time periodicity of the driving potential to express the wavefunction as the product of a phase and a periodic function in time, reducing the complexity to solve the time-dependent Schrödinger equation. Advances in Floquet methods have led to the development of Floquet perturbation theory in the form of the high-frequency and van-Vleck expansions [41, 42] where an effective time-independent Floquet Hamiltonian can be obtained. Such methods have been applied to Dirac semimetals [43], WSMs [41, 42], and even quantum spin liquids [44], to generate controllable transport properties.

In the context of transmission spectra, Fano resonances have been studied in many areas of physics since its inception in 1935 [45]. It is characterized by a perfect transmission followed by a total reflection or vice-versa,

* tanay.nag@hyderabad.bits-pilani.ac.in

† ♣SD, AM and RS contributed equally.

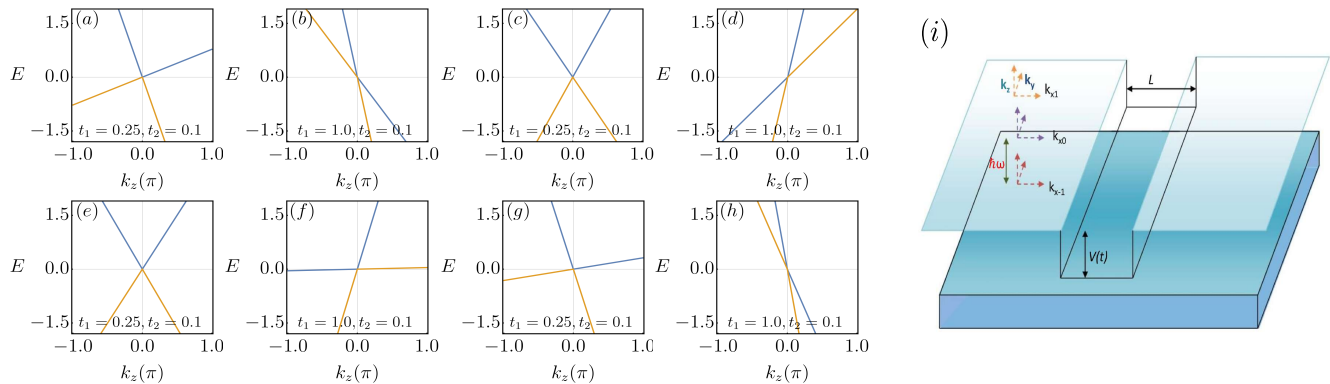


FIG. 1: The dispersion for the Hamiltonian in Eq. (1) are shown in (a-h). We consider $(\phi_1, \phi_2) = (\pi/4, \pi/2)$ and $(\pi, \pi/2)$ in (a,b) and (c,d) [(e,f) and (g,h)], respectively for $s = +1$ [$s = -1$]. The yellow and blue bands represent $E_{s,-}$ and $E_{s,+}$ as given in Eq. (3). We choose $t = t_z = 1$, $k_x = k_y = 0$ and $k_0 = \pi/2$. (i): The potential landscape is shown where the electron is transported in the x -direction through a harmonically driven potential $V(t) = -V_0 + V_1 \cos(\omega t)$ of width L . This potential landscape is only applicable along x -direction which is perpendicular to the direction of tilt. $\hbar\omega$ represents the photon energy for virtual processes, and k_{x_i} represent the various momenta for the Floquet sidebands with $i = -1, 0, 1$.

leading to an asymmetric resonance profile. The phenomenon can be explained by considering the interaction of localized states with a range of propagating continuum modes, wherein the transmission enhancement occurs due to constructive interference, and the reflection enhancement due to destructive interference, between different quantum trajectories. In the context of non-adiabatically driven quantum systems, Floquet sidebands are formed, and when one of these approaches a quasi-bound state, a Fano resonance occurs. Fano resonances have been noticed in various contexts such as for light propagation in photonic devices [46, 47], scattering in mesoscopic transport systems [46, 48–58] and superconducting Josephson junctions [46, 59], graphene [60], Dirac semimetals [61], and WSMs [62].

Previous literature has dealt with the Fano resonance structure of Dirac [61] and Weyl systems [63] employing Floquet theory in the presence of a harmonically driven potential well. However, there is not much commentary on the consequences of tilt in the energy dispersion on Fano resonances in these cases [64]. Considering the fact that tilt appears to be a key factor in manipulating the transport properties of WSMs as described previously [23–25], and motivated by the intricacies of Fano resonances, we examine the role of tilting on Fano resonances in three-dimensional WSMs in this work. In particular, we examine the Fano resonances, exploiting the Floquet scattering formalism, as a function of tilt strength on type-I and type-II WSMs and uncover hitherto unexplored physics in this context where tilt direction (say along z -axis) is transverse to the transport through the harmonically driven potential well (say along x -axis). Given a value of tilt momentum, we find that the Fano resonance energies depend linearly on tilt strength while the energy gap between two Fano resonances, ap-

pearing for two adjacent values of transverse momentum (say along y -axis) remains insensitive to the change in the tilt strength. On the other hand, given a value of transverse momentum, Fano resonance energies depend linearly on tilt strength and the corresponding tilt momentum in a coupled manner such that the energy gap between two Fano resonances, occurring for two adjacent values of tilt momentum, changes with the variation in the tilt strength. The exclusive (inclusive) behaviour between tilt strength and the transverse (collinear) momentum with respect to tilt direction is essentially caused by tilt-mediated and normal parts of the quasi-bound state energies inside the potential well. We also investigate the effect of chirality on the transmission spectra in the above cases. This allows us to understand the interplay between the tilt and Floquet scattering leading to the rich profile of Fano resonances through a harmonically driven potential well for 3D WSMs.

The structure of this manuscript is as follows: In Sec. II we consider the minimal model of a time reversal symmetry broken WSM with tilt, capable of hosting the type-I and type-II phases, and introduce the harmonically driven quantum well. Sec. III contains the solution to Schrodinger's equation and formulation of the S-matrix. We present the results for the transmission coefficients in Sec. IV for varying tilts, where the characteristic Fano resonances are demonstrated. A discussion on the results and the implications on future research is presented in Sec. V. We summarize our findings and conclude in Sec. VI.

II. MODEL AND TIME-DEPENDENT QUANTUM WELL

We begin our study by considering the low-energy minimal model Hamiltonian around a Weyl point of chirality s as given below [22]

$$H = 2k_z[t_1 \sin(\phi_1 - sk_0) + 2t_2 \sin(\phi_2 - 2sk_0)]\sigma_0 + t(\sigma_x k_x + \sigma_y k_y) + st_z \sigma_z k_z \sin k_0, \quad (1)$$

where $\sigma_x = \begin{pmatrix} 0 & 1 \\ 1 & 0 \end{pmatrix}$, $\sigma_y = \begin{pmatrix} 0 & -i \\ i & 0 \end{pmatrix}$ and $\sigma_z = \begin{pmatrix} 1 & 0 \\ 0 & -1 \end{pmatrix}$ are Pauli matrices. t_z and t are the spatially non-isotropic Fermi velocities of the Weyl points. Here the identity term causes a tilt along the k_z direction where $t_{1,2}$ denotes the parameters which control tilt strength. The phase factors $\phi_{1,2}$ represent the fluxes in hopping along z -direction in a lattice regularized model where the Weyl points appear at $(0, 0, sk_0)$. Note that the tilt term can be finite even when $\phi_{1,2} = 0$ indicating the fact that finite $t_{1,2}$ is essentially responsible for a tilted dispersion. The above model Eq. (1) can host type-I, type-II as well as hybrid phase where one Weyl point is type-I and its chiral counterpart is type-II. Once both the Weyl points can either be type-I or type-II, only one set of parameters, comprised of (t_1, ϕ_1) or (t_2, ϕ_2) only, is enough to give rise to the above phases where both the Weyl points are tilted in an identical manner usually. Importantly, for the hybrid phase, one usually needs two sets of parameters (t_1, ϕ_1) and (t_2, ϕ_2) such that two Weyl points can be tilted in different manner. However, the hybrid phase can only be supported by the lattice version of the model. In the present case, we restrict ourselves to the type-I and type-II phases as we consider an isolated Weyl point individually. Therefore, once can in principle adopt a simple form of the tilt term with only one set of parameters. We will demonstrate the upshot of the tilt term in the Fano resonance energy in Fig. 7 that may not be obvious from the simple form of tilt term.

The degree of tilt η_s for a given Weyl point of chirality s is defined as

$$\eta_s = \left| \frac{2[t_1 \sin(\phi_1 - sk_0) + 2t_2 \sin(\phi_2 - 2sk_0)]}{st_z \sin k_0} \right|. \quad (2)$$

This can be evaluated separately for each node to get the type-I ($\eta_s < 1$) and type-II ($\eta_s > 1$) WSM phases in general with $s = \pm 1$. $\eta_s = 1$ marks a Lifshitz phase transition which alters the nature of the Fermi surface as has been observed in the two phases. The dispersion relation, associated with the Hamiltonian Eq. (1), is given by

$$E_{s,u} = 2k_z[t_1 \sin(\phi_1 - sk_0) + 2t_2 \sin(\phi_2 - 2sk_0)] + u\sqrt{t^2(k_x^2 + k_y^2) + t_z^2 k_z^2 \sin^2 k_0}, \quad (3)$$

where $u = \pm$ represent the conduction and valence bands. The Hamiltonian hosts both type-I and type-II phases of WSMs as depicted in Figs. 1 (a-h). The band dispersion $E_{s,u}$ along the tilt momentum k_z for type-I and type-II phases are depicted in Figs. 1 (a,c,e,g) and (b,d,f,h), respectively.

We now choose to subject this system to a harmonically driven quantum well of width L in the x -direction. The potential $V(t)$ for the well is defined as [60, 64, 65],

$$V(t) = \begin{cases} -V_0 + V_1 \cos(\omega t) & |x| \leq L/2 \\ 0 & |x| > L/2 \end{cases} \quad (4)$$

where V_0 is the depth of the static potential well. V_1 and ω denote the amplitude and frequency of the harmonic drive. The setup of our system is shown in Fig. 1 (i), where the qualitative features of the driving potential in the three regions of interest are shown explicitly. The harmonically driven quantum well is confined to a region of width L in the x -direction, while such a potential landscape is absent in the z, y -directions. Note that there is no potential outside of the specified region $-L/2 < x < L/2$. The electron wavefunction is simply plane waves along the z, y -directions while x -component is non-trivial. It is very important to note that the tilt and the direction of flow of electrons are mutually perpendicular as this will have a significant role to play in our forthcoming results.

III. FLOQUET S-MATRIX

Let us define the wave function as a two-component spinor $\psi = \begin{pmatrix} \psi_1 \\ \psi_2 \end{pmatrix}$, and with this, we now solve Schrödinger's equation in the three regions described above employing the Floquet ansatz. First we consider the region $|x| > L/2$ and find an analytical expression for the wavefunction as follows

$$\psi = \begin{pmatrix} 1 \\ S_{\pm}(E) \end{pmatrix} \exp[\pm ik_x x + ik_y y + ik_z z], \quad (5)$$

where $S_{\pm}(E) = \frac{t(\pm k_x + ik_y)}{E - \tilde{t}k_z + st_z k_z \sin k_0}$ with $\tilde{t} = 2t_1 \sin(\phi_1 - sk_0) + 4t_2 \sin(\phi_2 - 2sk_0)$ and E represents the incident energy. This term is regarded as normalization of the wave-function. It is hence implied that $S_{\pm}(E)$ is a function of incident energy E , momentum $k_{x,y,z}$, tilt factor \tilde{t} , and t_z . However, for the ease of notation, we adopt the notation $S_{\pm}(E)$. In order to obtain the wavefunction for the potential region $-L/2 \leq x \leq L/2$, we replace E with $E - V_0$. This results in the substitution of k_x and $S_{\pm}(E)$ respectively with q_x and $S'_{\pm}(E) = S_{\pm}(E - V_0)$ within the above region. Solving the Schrödinger equation we find that the wavefunction for all spatial regions is [60, 65]

$$\psi_n = e^{-iEt/\hbar + ik_y y + ik_z z} \begin{cases} A_n^i N_{n+} \begin{pmatrix} 1 \\ S_+(E_n) \end{pmatrix} e^{ik_{xn}x} + A_n^o N_{n-} \begin{pmatrix} 1 \\ S_-(E_n) \end{pmatrix} e^{-ik_{xn}x}, & x < -L/2 \\ \sum_{m=-\infty}^{\infty} [a_m N'_{m+} \begin{pmatrix} 1 \\ S'_+(E_m) \end{pmatrix} e^{iq_{xm}x} + b_m N'_{m-} \begin{pmatrix} 1 \\ S'_-(E_m) \end{pmatrix} e^{-iq_{xm}x}] J_{n-m} \left(\frac{V_1}{\hbar\omega} \right), & -L/2 \leq x \leq L/2 \\ B_n^i N_{n-} \begin{pmatrix} 1 \\ S_-(E_n) \end{pmatrix} e^{-ik_{xn}x} + B_n^o N_{n+} \begin{pmatrix} 1 \\ S_+(E_n) \end{pmatrix} e^{ik_{xn}x}, & x > L/2 \end{cases} \quad (6)$$

Here $N_{n\pm} = \frac{1}{\sqrt{1+|S_{\pm}(E_n)|^2}}$ and $N'_{m\pm} = \frac{1}{\sqrt{1+|S'_{\pm}(E_m)|^2}}$ are the appropriate normalizing factors, and $A_n^{i(o)}$ and $B_n^{i(o)}$ are the amplitudes of the incoming (outgoing) waves, associated with n -th channel, at the left and right boundaries of the well. Note that $E_n = E + n\omega$ considering $\hbar = 1$. In Eq. (6), one can thus find $S_{\pm}(E_n) = \frac{t(\pm k_x + ik_y)}{E_n - ik_z + st_z k_z \sin k_0}$, $S'_{\pm}(E_n) = \frac{t(\pm k_x + ik_y)}{E_n - V_0 - ik_z + st_z k_z \sin k_0}$.

From fundamental quantum mechanical considerations, we demand continuity and differentiability of the wave function at the boundaries of the driving potential. This allows us to relate the incoming amplitudes with the outgoing amplitudes via the intermediate a_n and b_n amplitudes. The detailed derivation on the application of the boundary conditions is given in Appendix A. We proceed with the construction of the scattering matrix S . The scattering matrix is defined as [66],

$$\begin{pmatrix} A^o \\ B^o \end{pmatrix} = \begin{pmatrix} R & T' \\ T & R' \end{pmatrix} \begin{pmatrix} A^i \\ B^i \end{pmatrix} = S \begin{pmatrix} A^i \\ B^i \end{pmatrix} \quad (7)$$

where A^i and B^i represent the amplitudes of the incident waves and A^o and B^o represent the amplitudes of the outgoing signal. The reflection (R, R') and transmission (T, T') sectors of the S matrix can be represented as [65]

$$\begin{pmatrix} R & T' \\ T & R' \end{pmatrix} = \begin{pmatrix} r_{00} & r_{01} & \dots & t'_{00} & t'_{01} & \dots \\ r_{10} & r_{11} & \dots & t'_{10} & t'_{11} & \dots \\ \dots & \dots & \dots & \dots & \dots & \dots \\ \dots & \dots & \dots & \dots & \dots & \dots \\ t_{10} & t_{11} & \dots & r'_{10} & r'_{11} & \dots \\ t_{10} & t_{11} & \dots & r'_{10} & r'_{11} & \dots \\ \dots & \dots & \dots & \dots & \dots & \dots \\ \dots & \dots & \dots & \dots & \dots & \dots \end{pmatrix} \quad (8)$$

where r_{nm} and t_{nm} are reflection and transmission amplitudes for modes incident from the left and r'_{nm} and t'_{nm} are reflection and transmission amplitudes for modes incident from the right. The detailed derivation on S-matrix formulation is given in Appendix B. Here, we have $n, m \in (0, \infty)$ since only propagating modes are considered. Note that we consider only one incoming electron of energy E i.e., there exists only one incoming channel. Hence, we only work with $n = 0$ case. From the S matrix, we can define the total transmission coefficient T as [60, 64, 65]

$$T = \sum_{m=0}^{\infty} \frac{\text{Re}(k_0)}{\text{Re}(k_m)} |t_{0m}|^2. \quad (9)$$

m in Eqs. (6) and (9) are the same index on which the summation has to be performed. Note that m (n) represents Floquet sidebands (incoming channels) within (outside) the potential region in Eq. (6) whereas in Eq. (9), m represents the column index of the transmission matrix t_{nm} .

IV. RESULTS

We now proceed with the numerical evaluation of the transmission coefficient (T) and reflection coefficient (R) from the S -matrix. In all cases, we ensure that $R+T = 1$. We investigate the Fano resonance profile with the incident energy E by keeping k_z fixed and varying k_y in Figs. 2 and 3 for positive and negative chiralities, respectively. We further explore the Fano resonance characteristics by keeping k_y fixed and varying k_z in Figs. 4 and 5 for positive and negative chiralities, respectively. These investigations help us understand the tilt-mediated Fano resonance profile along the direction of tilt momentum and perpendicular to it. In all the above scenarios, we consider two sets of values $(\phi_1, \phi_2) = (\pi/4, \pi/2)$ and $(\phi_1, \phi_2) = (\pi, \pi/2)$ such that effect of the tilt is extensively analyzed. For our numerical computation, we choose $k_0 = \pi/2$, $t = t_z = 1$ and $s = \pm 1$, without the loss of generality. For $\phi_1 = \pi/4$ and $\phi_2 = \pi/2$, we obtain $\eta_{\pm} = |\sqrt{2}t_1 \pm 2\sqrt{2}t_2|$. We find $\eta_{\pm} = |4t_2 \mp 2t_1|$ for $\phi_1 = \pi$ and $\phi_2 = \pi/2$. We now choose appropriate values of t_1 and t_2 such that we are able to probe all phases of the WSM model. We reiterate that $\eta_{\pm} < 1$ represent type-I WSMs, and $\eta_{\pm} > 1$ represents type-II WSMs. Notice that $t_{1,2}$ are key parameters responsible for tilted spectrum even in the absence of $\phi_{1,2}$, i.e., $\phi_{1,2} = 0$.

The static potential well does not yield any Floquet side bands as there are no additional degrees of freedom that result in energy replication. In the case of the periodically driven potential well, there exists an additional degree of freedom namely, time period or frequency yielding the energy replication in terms of the frequency [38]. The Floquet theory allows us to probe the time-dependent problem in a time-independent man-

ner at stroboscopic time intervals after a complete time period. However, the time-independent Floquet Hamiltonian after a full period contains all the Fourier modes in the frequency space which enlarges the dimensionality of the problem by taking into account Floquet side bands. One can think of Floquet theory as the temporal analog of the Bloch theory where the spatially periodic array of potential barriers produces a periodic Bloch wave-function. Note that time period T (spatial periodicity of potential barrier a) introduces the repetitive nature of energy (wave-function) with frequency ω (wave-vector k) in the Floquet (Bloch) theory. The solution of the time-dependent Schrödinger equation takes the form $\psi(t) = e^{i\mu t}\phi(t)$ where quasi-states are periodic $\phi(t) = \phi(t + T)$ and μt is defined modulo $2\pi m$ with m being an integer. This further guarantees that quasi-energy μ is only well-defined up to the driving frequency ω at stroboscopic time intervals after a complete time period such that $\mu \in [-\omega/2, -\omega/2]$ and $\mu + m\omega$ is an equally valid quasi-energy solution. The finite values of $m \neq 0$ corresponds to the Floquet side bands. Connecting with the Bloch theorem, a generic time-independent wave-function can be written as $\psi(r) = e^{ikr}\phi(r)$ with $\phi(r + a) = \phi(r)$ and kr is defined modulo $2\pi m$. This causes the momentum k to be defined up to the reciprocal lattice vector $G = 2\pi/a$ such that $k = k + mG$. One can hence obtain the extended Brillouin zone of μ in the frequency space for the Floquet case which is just equivalent to the extended Brillouin zone of the wave-functions in the momentum space for Bloch theorem. This results in $\mu_m = \mu_0 + m\omega$ which m represents the multiple Floquet side bands.

The harmonically driven potential well leads to the formation of multiple copies of quasi-bound states in the potential region which are absent for the static potential well. The multiple copies of the quasi-bound state energies that are separated by the photon energy $\hbar\omega$ from each other can be alternatively thought of as quasi-bound Floquet sidebands where virtual photon transfer processes take place. Once the incident energy matches with any of these quasi-bound state energies, one encounters a Fano resonance. More precisely, when the energy difference between the incident beam and the quasi-bound state energy is an integer multiple of $\hbar\omega$, an electron can be absorbed into the quasi-bound state or an electron can be emitted from the quasi-bound state yielding the peak-dip or dip-peak profile of Fano resonance in transmission spectra. Note that the quasi-bound states are localized inside the potential region while their energies depend on the details of WSM and static potential depth V_0 . The concept of Floquet sidebands is also parallelly applicable to the incident and outgoing beams where their energies are multi-valued and separated by $\hbar\omega$ from each other. The Fano resonance can be equivalently considered as an outcome when the energy of the incident Floquet sideband matches with the quasi-bound states of the well. The relationship between the Fano resonance energy E_F i.e., the value of incident energy where Fano resonance

occurs and the quasi-bound state energy E_b is given by $E_F - E_b = n\hbar\omega$ where n can be positive or negative integer. Once we absorb $n\hbar\omega$ inside E_b (E_F), we refer to quasi-bound (incident) Floquet sidebands as described above. In what follows, we are interested in the distribution of the Fano resonances as we vary the different parameters described above. Our aim is to investigate the nature of E_b extensively by tuning the properties of WSM. It can be presumed that E_b incorporates the contribution from the tilt term of WSM as well.

In all cases, we work with the natural units $\hbar = c = e = k_B = 1$. This helps us to examine the Fano resonance in a simplified manner without altering the qualitative features. We choose $t_2 = 0.1$ for all our calculations. We consider one Floquet sideband around the zero photon-sector in our numerical analysis, which is sufficient to achieve numerical accuracy with a finite termination of the infinite sum. Note that $V_1/\omega \ll 1$ in our analysis. We consider incident energy, potential barrier height, and frequency all in the unit of 10^{-3} eV. The Fermi velocities t, t_z and tilt strength $t_{1,2}$ are measured in the unit of 10^6 m/s. The momenta $k_{y,z}$ are considered in units of 10^{-9} m $^{-1}$. The length of the potential barrier L is in units of 10^{-9} m. One can increase L and consider it in units of L^{-6} m but the transmission spectra remain qualitatively unaltered [61, 62, 64]. The above choices of the parameters restrict the low-energy model, described in Eq. (1), to have energy in the meV regime. This is consistent with the long wave length limit where the lattice spacing a is considered in the units of m such that $k \ll 10^0$ m $^{-1}$. On the other hand, the dimension of the system in the tilt direction along z -axis $L_z \sim 1/k_z$ is large compared to the barrier width along the transport direction i.e., x -direction: $L_z > L$. We do not need to satisfy such condition along y -direction as the tilt is only along z -direction. However, more importantly, the choice of L has to be comparable to the meV energy scale that we always satisfy. We further note that the Fano resonances are not limited by a particular choice of the above unitful parameters. Their quantitative features can be altered, however, qualitative behavior remains unchanged. Therefore, the validity of our findings, presented below, is intact as far as the low-energy model of WSM is concerned.

A. Case 1: Fixed k_z and varying k_y

We examine the evolution of the transmission spectra in Figs. 2 and 3 for $s = 1$ and -1 , respectively, and when the tilt factor t_1 increases such that we encounter type-I and type-II WSM phases. The details of the Fano resonance energies are given in table I.

The Fano resonances for the larger k_y appear at greater values of incident energy E irrespective of the choice of the parameters $\phi_{1,2}$, $t_{1,2}$ and chiralities $s = \pm 1$ as clearly observed by scrutinizing the first Fano resonance in Figs. 2 (a,b,e,f) and 3 (a,b,e,f). However, we observe signifi-

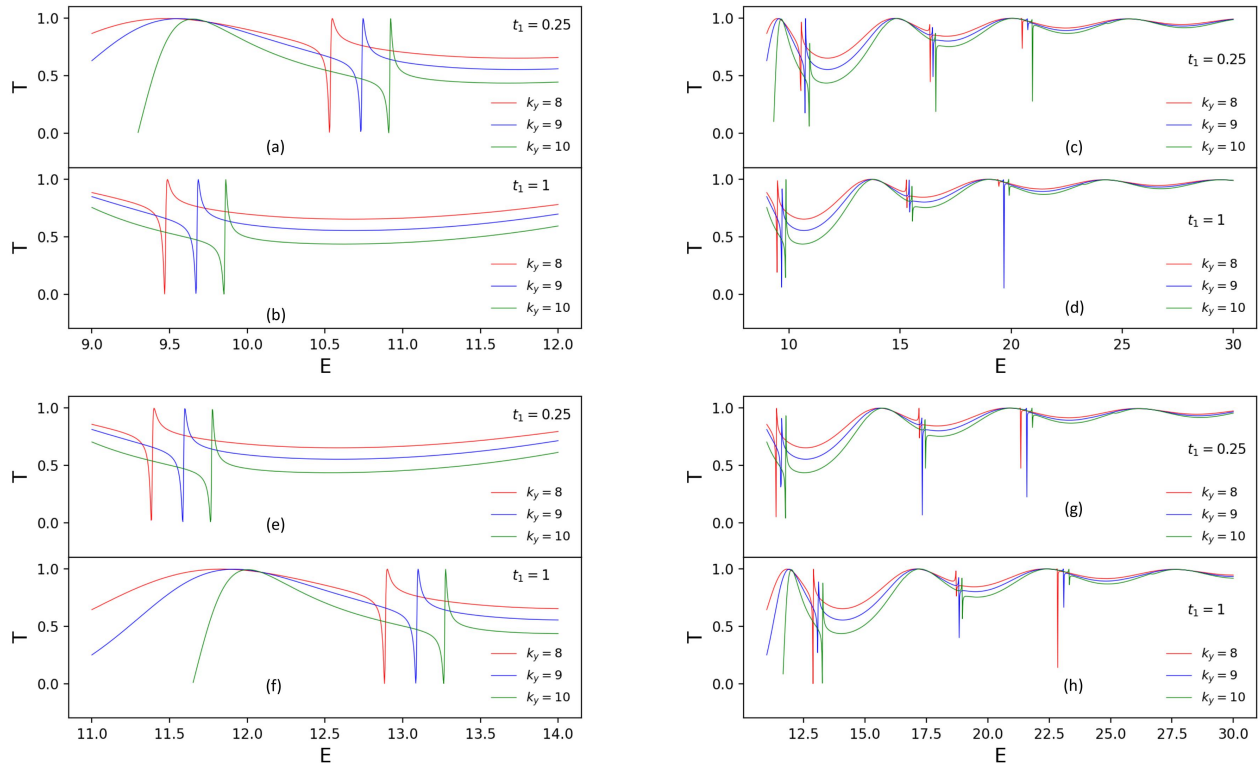


FIG. 2: Transmission spectra T , computed from Eq. (9), as a function of incident energy E for positive chirality Weyl point with $s = +1$ are shown above keeping k_z fixed while changing value of k_y . Here (a,b) depict first Fano resonance and (c,d) show a large region of incident energy region for $\phi_1 = \pi/4$ and $\phi_2 = \pi/2$. We repeat the plots (a,b) and (c,d) in (e,f) and (g,h), respectively for $\phi_1 = \pi$ and $\phi_2 = \pi/2$. Parameters are taken as follows $L = 0.6$, $k_z = 1$, $V_0 = 100$, $V_1 = 1$ and $\omega = 15$.

(ϕ_1, ϕ_2)	s	t_1	1 st Fano Resonance Energy			η_s
			$k_y = 8$	$k_y = 9$	$k_y = 10$	
$(\pi/4, \pi/2)$	1	0.25	10.54	10.74	10.92	0.6364
		1	9.48	9.68	9.86	1.6971
	-1	0.25	11.24	11.44	11.62	0.0707
		1	12.31	12.51	12.68	1.1314
$(\pi, \pi/2)$	1	0.25	11.39	11.60	11.77	0.1
		1	12.89	13.09	13.27	1.6
	-1	0.25	10.39	10.49	10.77	0.9
		1	8.89	9.09	9.27	2.4

TABLE I: Energies associated with Fano resonances for type I ($\eta_s < 1$) and type II ($\eta_s > 1$) WSMs for both the chiralities $s = \pm 1$ (with $k_z = 1$ for case 1).

cant differences between the cases $s = 1$ and $s = -1$ as described below. The Fano resonance energy decreases with t_1 for the $s = 1$ case and increases with the increase in t_1 in $s = -1$ case, for $(\phi_1, \phi_2) = (\pi/4, \pi/2)$. An opposite trend is noticed for $(\phi_1, \phi_2) = (\pi, \pi/2)$ case. The underlying physics is explained by noting that varying the tilt alters the energies of the quasi-bound Floquet

states, which leads to changes in the energetics of the Fano resonances - hence they appear at different points as a function of tilt. A complete closed form expression the quasi-bound state energy E_b is very useful to understand the emergence of the Fano resonances. One can naively anticipate the tilt dependence in the above quantity to be identical to the tilt term in energy of the bare Hamiltonian. This we shall investigate below extensively. Passing by, we note that the quasi-bound state energies for the untilted and the tilted case differ by the tilt term precisely.

Examining the first Fano resonance at energy E_F^1 further, we find that the Fano resonance energy linearly increases with increasing k_y irrespective of the chirality of the node and tilt strength. This causes the gap between Fano resonance energies, occurring for two different values of k_y to become constant irrespective of the choice of parameters $\phi_{1,2}$, $t_{1,2}$ and chiralities $s = \pm 1$. This clearly conveys that the tilt-mediated part in the quasi-bound state energy is not a function of k_y . One can decompose the quasi-bound state energy E_b in two parts where the tilt-mediated part E_b^t vanishes if $t_{1,2} = 0$ while the untilted normal part E_b^n remains non-zero even if $t_{1,2} = 0$; $E_b = E_b^t + E_b^n$. This is qualitatively similar to the static

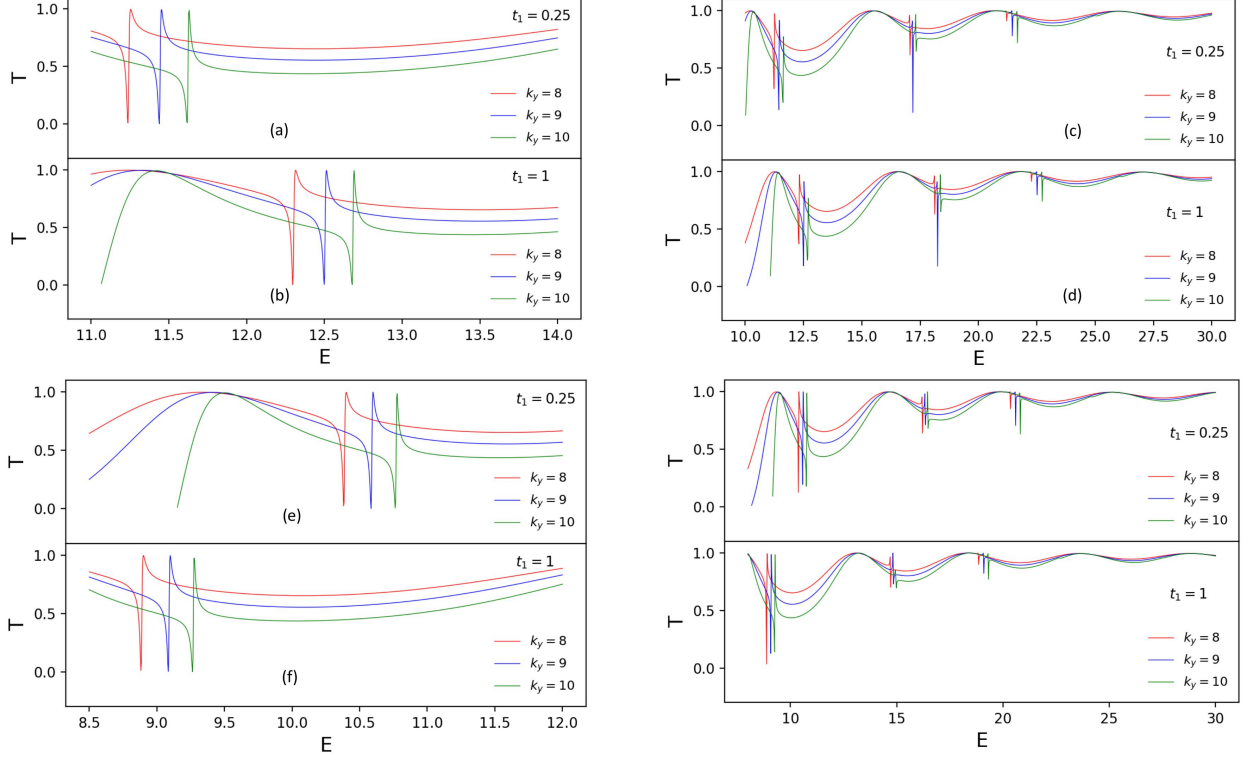


FIG. 3: Variation of T as a function of the incident energy E for negative chirality Weyl point with $s = -1$. Fig. 2 is repeated here for $s = -1$, keeping all other parameters same.

case Eq. (3) where $t_{1,2}$ are responsible for the tilt even in the absence of $\phi_{1,2}$. Importantly, the k_y -dependency comes solely from the untilted part of the quasi-bound state energy. This is also similar to the case of the static energy dispersion where the untilted part depends only on k_y while the tilted part is independent of k_y .

Interestingly, the tilt-mediated part E_b^t in the quasi-bound state energy is a function of $t_{1,2}$, $\phi_{1,2}$ and chirality leading to a change in quasi-bound state energy with all the above parameters while k_y is still kept fixed. This causes the Fano resonance energies to shift with all the above parameters [see Figs. 2 (a,b,e,f) and 3 (a,b,e,f)]. One can compute the tilt term as $2k_z(-st_1 \cos \phi_1 - 2t_2 \sin \phi_2)$, provided $k_0 = \pi/2$, from the static energy dispersion for all the above parameters to find a quantitative agreement with the shift in the Fano resonance energy. For example, the tilt term in the static case becomes more negative [positive] when t_1 increases for $(\phi_1, \phi_2) = (\pi/4, \pi/2)$ [$(\pi, \pi/2)$] and $s = +1$. On the other hand, the untilted part of quasi-bound state energy remains unaltered as it is independent of the tilt parameters $t_{1,2}$, $\phi_{1,2}$. Therefore, the quasi-bound state energy will be shifted by the exact amount as the tilted part of the static energy, demonstrated in Fig. 2 (a,b,e,f). This correlation can be further verified for $s = -1$ with $(\phi_1, \phi_2) = (\pi/4, \pi/2)$ [$(\pi, \pi/2)$] where static tilt term increases in the positive [negative] energy side causing the

Fano resonance energy to increase [decrease] with t_1 [see Fig. 3 (a,b,e,f)]. One could expect all the above findings to be qualitatively remained if t_2 is varied while keeping t_1 fixed as the tilt term involves t_1 and t_2 both. Therefore, the tilt-mediated part of the quasi-bound energy states is exactly given by the static counterpart i.e., $E_b^t = 2k_z(-st_1 \cos \phi_1 - 2t_2 \sin \phi_2)$ with $k_0 = \pi/2$, while the untilted part E_b^n is anticipated to be a function of the barrier height V_0 , barrier width L , momenta $k_{y,z}$, and Fermi velocities t, t_z . A closed form expression, derived in Appendix D, suggests the lowering of the barrier height independent part of E_b^n as L increases.

We depict the follow-up Fano resonances, namely higher Fano resonances appearing at higher incident energies E_F^n with $n > 1$ after the first Fano resonance, for both the chiralities in Figs. 2 (c,d,g,h) and 3 (c,d,g,h). We notice that the energy gap between two consecutive Fano resonances always decreases for a given value of k_y when the incident energy becomes greater. This is essentially caused by the fact that the quasi-bound state energies are not equispaced, rather the energy gap between them decreases. These quasi-bound state energy levels inside the potential well take part in the virtual photon transfer process with the incident beam. The dip-peak structure in the following Fano resonances can be altered as compared to the first Fano resonance. We note that since there is no Fermi surface based phenom-

ena in this scattering analysis that even if we increase the tilt strength, our results do not distinguish between the type-I and type-II phases of WSM. The underlying physics is governed by the tilt altering the energies of the quasi-bound Floquet states, which leads to the changes in the energetics of the Fano resonances. As a result, they appear at different points as a function of tilt.

B. Case 2: Fixed k_y and varying k_z

Similar to the earlier subsection, we examine the evolution of the transmission spectra in Figs. 4 and 5 for $s = 1$ and -1 , respectively, when the tilt factor t_1 increases. The Fano resonance energies are listed in table II. Having examined the tilt-mediated effect in T by varying k_y , we here further scrutinize the explicit form of E_b^t , as already predicted earlier, with respect to k_z .

(ϕ_1, ϕ_2)	s	t_1	1 st Fano Resonance Energy			η_s
			$k_z = 0.8$	$k_z = 1$	$k_z = 1.2$	
$(\pi/4, \pi/2)$	1	0.25	11.06	10.92	10.77	0.6364
		1	10.21	9.85	9.49	1.6971
	-1	0.25	11.63	11.62	11.61	0.0707
		1	12.48	12.68	12.89	1.1314
$(\pi, \pi/2)$	1	0.25	11.75	11.77	11.79	0.1
		1	12.94	13.26	13.59	1.6
	-1	0.25	10.93	10.76	10.56	0.9
		1	9.74	9.26	8.79	2.4

TABLE II: Energies associated with Fano resonances for type I ($\eta_s < 1$) and type II ($\eta_s > 1$) WSMs for both the chiralities $s = \pm 1$ (with $k_y = 10$ for case 2).

The first Fano resonance energy E_F^1 , corresponding to positive chirality, decreases [increases] with increasing t_1 with a given value of k_z for $(\phi_1, \phi_2) = (\pi/4, \pi/2)$ [$(\pi, \pi/2)$] as depicted in Figs. 4 (a,b,e,f). The situation is reversed for negative chirality as shown in Figs. 5 (a,b,e,f). This feature is also observed in the previous case. On the other hand, the marked difference for the present case is the following: the energy gap between two successive Fano resonances, associated with two different values of the tilt momentum k_z , varies with increasing t_1 . This energy gap also changes if one changes the chirality as well as $\phi_{1,2}$. This suggests that the tilt-mediated part E_b^t in the quasi-bound state energy depends on k_z , $t_{1,2}$, $\phi_{1,2}$ and s . This can be quantitatively understood from the tilted part in the static energy dispersion Eq. (3). As discussed earlier, the untilted part E_b^n of the quasi-bound state energy is independent of $t_{1,2}$, $\phi_{1,2}$ and s . The tilt momentum k_z appears both in the tilted as well as untilted part of the above energy. Therefore, once we vary all the parameters $t_{1,2}$, and $\phi_{1,2}$ including k_z for a given chirality, both the untilted and tilted-mediated parts in the quasi-bound state energy change in a non-trivial manner.

The above phenomena lead to a rich Fano resonance profile that is an admixture of effects coming from tilt factors $t_{1,2}$ and tilt momentum k_z simultaneously. This can be further understood from the fact that beyond a certain value of t_1 the order of the Fano resonance with k_z changes i.e., quasi-bound state energies increase (decrease) with increasing k_z instead of decrease (increase). This is noticed in Fig. 5 (a,b). Therefore, the appearance of Fano resonances with k_z is relative to the choice of the parameters such as $t_{1,2}$, and $\phi_{1,2}$. One could expect similar findings if t_2 is varied while keeping t_1 fixed as the tilt term involves t_1 and t_2 both. A careful investigation suggests that the Fano resonance energy changes linearly with increasing k_z (t_1) for a given value of t_1 (k_z). This causes the energy separation between two subsequent Fano resonances to vary linearly with increasing the product of t_1 and k_z . This collective behavior indicates that tilt-mediated part of the quasi-bound state energies behave in a qualitatively different manner as compared to the untilted counterpart.

We now turn our attention to the follow-up Fano resonance at energies E_F^n with $n > 1$ profiles when the incident energy increases as shown in Figs. 4 (c,d,g,h) and 5 (c,d,g,h) for positive and negative chiralities, respectively. Similar to the earlier section, we find that the energy gap between two successive higher Fano resonances decreases with increasing the incident energy for a given value of k_z . Such repeated occurrence of Fano resonances with a variation in the dip-peak structures is commonly visible when t_1 increases as expected. The existence of multiple quasi-bound states with unequal energy spacing can be inferred as well from the above findings.

V. DISCUSSION

Previously we discussed the explicit form of E_b^t for a given value of t_1 while varying either collinear momentum k_z or transverse momentum k_y . In this section, we show that the specific form of E_b^t predicted from the earlier discussion is not special with respect to the values of t_1 chosen earlier. The expression of $E_b^t = 2k_z(-st_1 \cos \phi_1 - 2t_2 \sin \phi_2)$ with $k_0 = \pi/2$ is generic and not limited to a special range of $t_{1,2}$ and $\phi_{1,2}$. In order to strengthen our findings on the tilt-mediated part of quasi-bound state energy, we examine the evolution of Fano resonance energy E_F with t_1 as described below.

In particular, we plot the incident energies E_F^1 , corresponding to the first Fano resonance, as a function of t_1 keeping k_y as a parameter (see Fig. 6). We investigate the case of $(\phi_1, \phi_2) = (\pi/4, \pi/2)$ [$(\pi, \pi/2)$] in Fig. 6 (a,b) [(c,d)]. We repeat Fig. 6 with k_z as a parameter in Fig. 7. The linear behavior of Fano resonance energy with t_1 infers that the quasi-bound state energy varies linearly with t_1 .

This further boils down to the fact that the tilt-mediated part shows linear dependence with t_1 . The

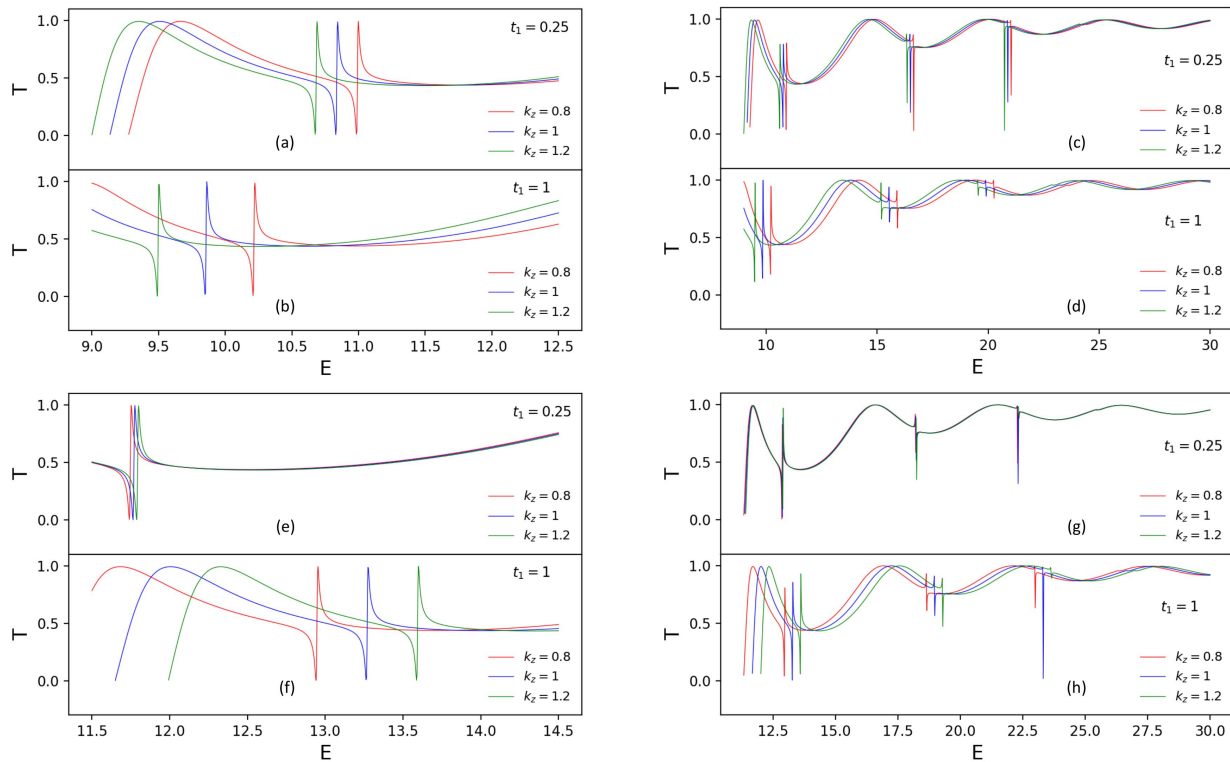


FIG. 4: Transmission spectra T , computed from Eq. (9), as a function of incident energy E for positive chirality Weyl point with $s = +1$ are shown above keeping k_y fixed while changing value of k_z . Here (a,b) display the first Fano resonance and (c,d) show a large energy region of incident energy for $\phi_1 = \pi/4$ and $\phi_2 = \pi/2$. We repeat (a,b) and (c,d) in (e,f) and (g,h), respectively for $\phi_1 = \pi$ and $\phi_2 = \pi/2$. Parameters are taken as follows $L = 0.6$, $k_y = 10$, $V_0 = 100$, $V_1 = 1$ and $\omega = 15$.

parallel straight lines, on the other hand, for different values of k_y suggests that the quasi-bound state energies change in an identical manner with k_y irrespective of the values of t_1 . This is in accordance with the fact that tilt-mediated part E_b^t of quasi-bound state energy does not depend on k_y . Interestingly, the untilted part of the above energy is expected to vary linearly with k_y as evident from the equidistant parallel lines. The parallel nature of the straight lines confirms that the energies of the quasi-bound state do not involve any product term $t_1 k_y$, rather it depends on k_y and t_1 separately.

The positive and negative slopes of these parallel lines denote the coefficient in front of these energies that depend on chirality as well as the choice of $\phi_{1,2}$. We find the sign of the coefficient reverses as chirality switches its sign while $\phi_{1,2}$ are kept fixed. The change in the sign of chirality $s = 1$ to $s = -1$ can alter the sign of the slopes of these straight lines without affecting their parallel nature. This further suggests that energies depend on the product of st_1 while k_y does not couple with s . One can understand all of the above findings by analyzing the tilt term $2k_z(-st_1 \cos \phi_1 - 2t_2 \sin \phi_2)$ in the static energy dispersion with a given set of parameters.

Examining Figs. 7(a,b) and (c,d) for $(\phi_1, \phi_2) =$

$(\pi, \pi/2)$ and $(\pi/4, \pi/2)$ respectively, we find that the first Fano resonance energy E_F^1 changes linearly with tilt parameter t_1 while the slope depends on k_z . This results in intersecting straight lines for different values of k_z unlike the previous case of parallel lines in Fig. 6. On the other hand, these energies also depend linearly on k_z given a fixed value of t_1 . Interestingly, for certain values of t_1 , the Fano resonance energies for different values of k_z become identical. This equi-energy point changes to a different value of t_1 once t_2 and/or the chirality s changes for a fixed parameter set of $\phi_{1,2}$. This refers to the fact that there exists an additional $t_2 k_z$ tilt term in the energy, and can be clearly understood from the tilt term $2k_z(-st_1 \cos \phi_1 - 2t_2 \sin \phi_2)$ of the static model. The intersection point is observed when the tilt-mediated part of the quasi-bound state energy vanishes i.e., $E_b^t = 0$ for a certain set of t_1^* and t_2^* values given $\phi_{1,2}$ fixed. The values of $t_{1,2}^*$, such that $-st_1^* \cos \phi_1 = 2t_2^* \sin \phi_2$, can be exactly computed from the tilt term in the static model.

The non-parallel intersecting nature of the straight lines confirms that energies of the quasi-bound state involve the product term $st_1 k_z$. This collective dependence rules out the individual dependence on k_z and t_1 . The change in the sign of chirality $s = 1$ to $s = -1$ alters the

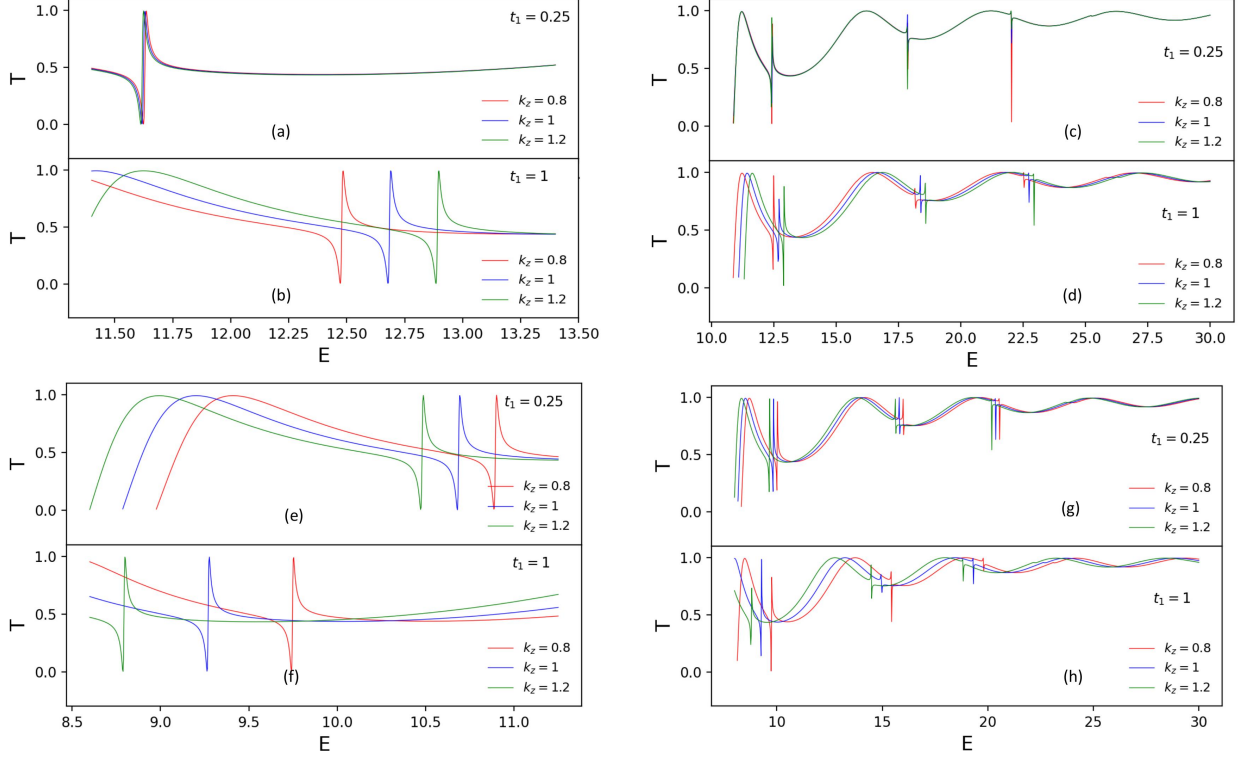


FIG. 5: We repeat Fig. 4 for negative chirality Weyl point with $s = -1$.

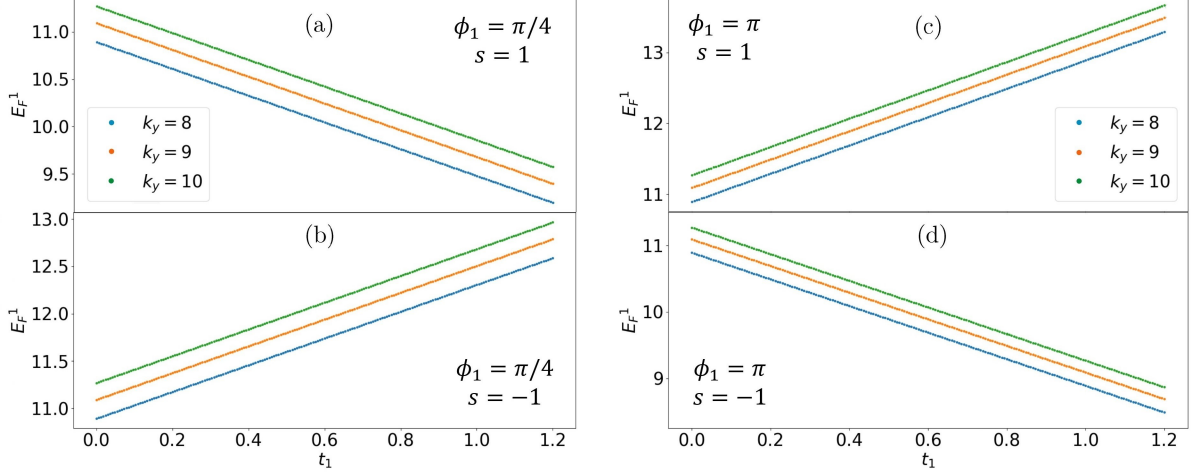


FIG. 6: The energy E_F^1 corresponding to first Fano resonance as found in Figs. 2 and 3, are shown as a function of t_1 . We consider $(\phi_1, \phi_2) = (\pi/4, \pi/2)$ and $(\pi, \pi/2)$ for (a,b) and (c,d), respectively. We choose $s = +1$ and -1 for (a,c) and (b,d), respectively. Parameters are taken as follows $L = 0.6$, $k_z = 1$, $V_0 = 100$, $V_1 = 1$ and $\omega = 15$.

sign of the slopes of these straight lines without affecting the intersecting nature. The energies change linearly with k_z while the proportionality factor depends on the product of st_1 and t_2 separately as evident from the tilt term in the low-energy Hamiltonian Eq. (1). This describes the intersecting nature of the plots and alteration in order of the Fano resonance peaks with k_z upon chang-

ing t_1 across t_1^* keeping all the other parameter fixed, as noticed in Fig. 5 (a,b).

Having discussed the parameter dependent response in Figs. 6 and 7, we here analyze the intersecting nature of E_F^1 profiles with respect to the tilt orientation of Weyl points. Once the tilt term changes from positive to negative values the intersecting point in t_1 can be observed

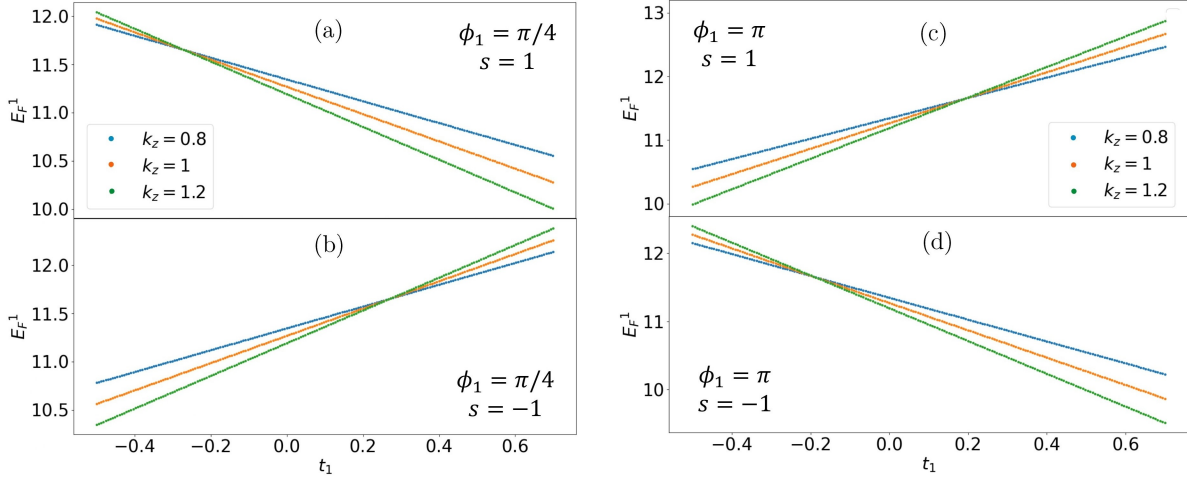


FIG. 7: The energy E_F^1 corresponding to first Fano resonance as found in Figs. 4 and 5, are shown as a function of t_1 . We consider $(\phi_1, \phi_2) = (\pi, \pi/2)$ and $(\pi/4, \pi/2)$ for (a,b) and (c,d), respectively. We choose $s = +1$ and -1 for (a,c) and (b,d), respectively. Parameters are taken as follows $L = 0.6$, $k_y = 10$, $V_0 = 100$, $V_1 = 1$ and $\omega = 15$.

when E_F^1 curves for different values of k_z meet. The order of E_F^1 curves for different k_z gets reversed once the intersecting point is met at $-st_1^* \cos \phi_1 = 2t_2^* \sin \phi_2$ irrespective of the chirality. One interesting observation is that for $|t_1| < |2t_2 \sin \phi_2 / \cos \phi_1|$, both chirality Weyl points share identical tilt orientation profiles. This is evident from the identical nature of the order of E_F^1 curves associated with k_z for both $s = \pm 1$ in 7 (a,b) and (c,d) with $(\phi_1, \phi_2) = (\pi/4, \pi/2)$ and $(\pi, \pi/2)$, respectively. On the other hand, for $|t_1| > |2t_2 \sin \phi_2 / \cos \phi_1|$, opposite chirality Weyl points show opposite tilt orientation profiles as the orders of E_F^1 curves get reversed with k_z outside the window of $-2t_2 \sin \phi_2 < t_1 \cos \phi_1 < 2t_2 \sin \phi_2$ for $s = \pm 1$. Therefore, the choice of the tilt term, considered here, allows us to have two opposite tilted Weyl points in a certain parameter regime.

This results in the fact that without altering the tilt term manually, we can probe the Fano resonance energy, associated with opposite tilted Weyl points, with tilt strength. This is markedly different from a simple tilt term, governed by a single set of parameter i.e., either by (t_1, ϕ_1) or (t_2, ϕ_2) , that does not necessarily yield two different tilt orientations among two opposite chirality Weyl points. A simplified tilt term with tilt momentum k_z and one set of parameters (t_1, ϕ_1) can also partially mimic the same results presented in Figs. 6 and 7 when the tilt orientations of Weyl points are manually made opposite to each other. Our choice of the tilt term is solely responsible for the interesting nature of E_F^1 lines for different values of the tilt momentum k_z . The tilt orientations for both the opposite chirality Weyl points can be simultaneously controlled by the two sets of parameters (t_1, ϕ_1) and (t_2, ϕ_2) and hence it does not require any manual tuning. This leaves recognizable change in the Fano resonance profile with tilt strengths while adopting a generalized form of the tilt term. In other words,

the orientation of tilt-driven intersecting points and their distinct locations in terms of tilt strength for different chirality are the key signatures of the particular tilt term considered here. Importantly, by varying t_1 it is possible to obtain the type-I, type-II and hybrid phase where one Weyl point is type-I and its chiral counterpart is type-II [22]. However, distinct signature of the above phases may not be obvious from E_F^1 lines. Nevertheless, the tilt term, considered here, has all these ingredients leading to tilt orientation mediated distinct transport response for opposite chirality Weyl points. Our findings are thus more general compared to that of a conventional tilt term.

The interference between the open (continuum states) and closed (Floquet sidebands) channels leads to Fano resonance where bound state energy plays a crucial role. The bound state energy is not simply given by the energy dispersion of the Weyl semimetal rather it is given by

$$E_b = \left[V_0 \pm \sqrt{(2l+1)^2 \frac{\pi^2 t^2}{4L^2} + t^2 k_y^2 + t_z^2 k_z^2 \sin^2 k_0} \right] + k_z \tilde{t} \quad (10)$$

with $\tilde{t} = 2t_1 \sin(\phi_1 - sk_0) + 4t_2 \sin(\phi_2 - 2sk_0)$ and $l = 0, \pm 1, \pm 2, \dots$. The barrier width and height are also important to determine the bound state energy. The tilt-independent part is thus given by $E_b^n = V_0 \pm \sqrt{(2l+1)^2 \frac{\pi^2 t^2}{4L^2} + t^2 k_y^2 + t_z^2 k_z^2 \sin^2 k_0}$ while the tilt-mediated part is $E_b^t = k_z \tilde{t}$ as predicted by our prior analysis with $k_0 = \pi/2$. The detailed derivation on S-matrix formulation is given in Appendix D. When the incident energy E matches with the bound state of the Floquet sidebands $E_b + n\omega$ (with $\hbar = 1$, and $n = 0, \pm 1, \pm 2, \dots$), we find Fano resonance at $E = E_F = E_b + n\omega$. Note that barrier height V_0 is absorbed within E_b . This is the reason that a simple kinematic relation between E_F and the energy dispersion, given by $E_F + n\omega = \tilde{E}(q_x, k_y, k_z, V_0)$

can describe the emergence of Fano resonance [65]. Note that $\tilde{E}(q_x, k_y, k_z, V_0)$ is not exactly given by the bulk energy dispersion in the presence of the static potential well which is found to be $\tilde{E}_{s,u} = E_{s,u} + V_0$ with $E_{s,u} = \tilde{t}k_z + u\sqrt{t^2(k_x^2 + k_y^2) + t_z^2k_z^2 \sin^2 k_0}$ and $u = \pm$. The potential effectively modifies k_x to q_x as $q_x = 2\pi m/L$ in E_b while the other terms inside the square root are proportional to $k_{y,z}^2$ and are exactly the same as that of the bulk energy dispersion. The tilt term appears in an identical way for \tilde{E}_b and $\tilde{E}_{s,u}$. Therefore, $\tilde{E}(q_x, k_y, k_z, V_0)$ can only be regarded as $\tilde{E}_{s,u}$ if $k_x \equiv q_x = 2\pi m/L$. The kinematic relation essentially dictates the shapes of the transmission of spectra at Fano resonances that are universal either exhibiting a peak followed by a dip or vice versa irrespective of the details of the underlying model. The increase (decrease) in the barrier length L reduces (enhances) the energy of the quasi-bound state resulting in the shift of Fano resonances as incident energy E varies.

We now discuss the impact of the underlying three-dimensional dispersion of WSM on the transmission spectra. In addition to the one(two)-dimensional problem, here we have momenta $k_{y,z}$ transverse to the propagation direction along x -axis. As a result, we have better tunability on the location of Fano resonance while their profiles are studied in Figs. 2, 3, 4, and 5 by varying k_y and k_z in a respective manner. To be precise, the parallel (intersecting) nature of Fano resonance energy with tilt strength t_1 in Fig. 6 (Fig. 7) is due to the fact that tilt momentum is unaltered (varied). These features are not very obvious from the earlier one- and/or two-dimensional studies [60, 65] revealing an intriguing manifestation of the tilt in the energy dispersion.

It is difficult to differentiate between the type-I/under-tilted and type-II/over-tilted WSM as Fermi surface physics is not captured from our analysis. In order to apprehend the change in the shape of Fermi pocket into the transmission spectra, one has to invoke the concept of chemical potential. In addition to the incident energy E , the bias voltage between the left and right sides of the potential well μ_L and μ_R can be considered to investigate the distinct transmission profiles caused by point-like and pocket-like Fermi surface. The parallel (intersecting) nature of the Fano resonance energy with tilt strength in Fig. 6 (Fig. 7) can be altered for different choices of gate voltage in the presence of leads. The variation with chemical potential i.e., gate voltage can serve as another possible route to differentiate between type-I and type-II WSM. This is a limitation of our present work that we leave open for future exploration by considering an appropriate Landauer-Büttiker version of the three-dimensional lattice Hamiltonian of WSM.

The Fano resonance spectral profile is characterized by energy shift F , spectral width Γ and an asymmetry parameter q [67, 78, 79]. The first two terms of F and Γ are real and imaginary parts, respectively, of a self-energy of the scattering system in question. The coupling be-

tween the open and closed channels, lying outside and inside the potential regions respectively, can be regarded as V_E . To be precise, V_E is represented by V_1 multiplied by an overlap between the associated discrete and continuum wavefunctions in the x -direction. Importantly, q depend on $|V_E|^2$ and a phase factor of V_E . The Fano peak position is associated with the extremum of the first derivative of the scattering phase shift with respect to E . This is related to the time-delay matrix as obtained from scattering theory. One can anticipate the spectral width Γ of the Fano peak from the above the derivative rule. One can also obtain q qualitatively by fitting the appropriate formula with regard to the relevant channels [67]. It would be interesting to study the energy shift F and asymmetry parameter q from the scattering matrix formalism in future. However, we can comment that the sharpness of the resonance structure is affected by the tilt term as noticed in Figs. 2, 3, 4, and 5.

Controlling material parameters in general is considered tricky in the experimental community as the tilt can easily be intrinsically present in Dirac semimetals and WSMs with linear as well non-linear band dispersion [22]. We, however, point out a few ways in which our results may be tested in a laboratory. Given the fact that uniaxial strain is found to be useful to introduce tilt in the energy dispersion of graphene [68], applying strain can also cause a variation in the tilt of the WSMs. This method relies on altering the spatial and temporal components of the gauge field [69–71] and maybe used to find Fano resonances when driven by a laser field. Another way in which tilt variations appear is through periodic driving, which has been reported to produce type-I and type-II WSMs [72]. Notice that the tilted Dirac dispersion has been predicted to appear in two-dimension for quinoid-type [73] and hydrogenated graphene [74], 8-Pmmn Borophene [75], planar arrays of carbon nanotubes [76]. The tilted Dirac cones have been experimentally observed in photonic Lieb-kagome lattices [77]. We believe that the above theoretical predictions and experimental techniques will be instrumental in future to engineer the tilted dispersion of WSMs in three-dimension.

VI. CONCLUSION

In this work, we consider harmonically driven quantum well to study the Fano resonances in tilted WSMs by investigating the transmission spectra using the Floquet scattering theory technique. The potential is oriented in the transverse direction with respect to the tilt allowing us to study the transmission by varying momentum along and perpendicular to the tilt direction. Our study sheds light on the effect of tilt on the Fano resonance where the Fano resonance energy changes linearly with tilt strength. This is caused by the tilt-mediated part of the energy associated with the quasi-bound state residing inside the potential well. For fixed value of the collinear (transverse) momentum with respect to the tilt direction,

the energy difference between two Fano resonances, appearing for two adjacent values of transverse (collinear) momentum, does not (does) change with tilt strength. This finding clearly indicates that collinear (transverse) momentum is coupled (decoupled) with tilt strength in the tilt-mediated part of the quasi-bound state energy. The variation of the first Fano resonance energy with tilt strength further confirms that the tilt-mediated part of the above energy is the same as the tilt term present in the static energy dispersion. We investigate the evolution of transmission profile with respect to the other tilt parameters and chirality of the Weyl points extensively, from which we exact form of the tilt-mediated part is further verified. The normal part of the quasi-energy spectrum is dependent on the collinear as well as the transverse momentum resulting in the rich profile of Fano resonance in the parameter space.

Our work thus uncovers the complex interplay between the tilt and Fano resonance by probing the tilt-mediated part of quasi-bound state energy. while the closed form of the later yields significant insight to understand the numerical results. The generic form the tilt term allows us to explore the tilt orientation mediated response of the

Weyl points that is not usually captured by conventional tilt terms. We believe that our study might play an important role in understanding the experimental findings such as currents for periodically driven systems as far as the microscopic mechanisms are concerned. In real mesoscopic systems, the potential region is confined in a finite region of space and hence edge effects are important. Therefore, it would be interesting to study the edge effects in these systems. At the same time, the dynamics of Fano resonance under magnetic field, disorder, interaction and other dephasing mechanism might be important for future studies.

VII. ACKNOWLEDGEMENT

We acknowledge the technical help from Rui Zhu. TN would like to thank Ipsita Mondal for the initial discussions on the Floquet scattering techniques. TN also thanks Anton Gregefalk for fruitful discussions. TN acknowledges NFSG “NFSG/HYD/2023/H0911” from BITS Pilani.

Appendix A: Boundary matching

In this appendix, we discuss the boundary conditions in details for the wave-functions to be continuous across the boundary along with their derivations. This allows us to relate the coefficients A_n , B_n , a_m and b_m as discussed in Sec. III.

Applying the boundary condition $x = -L/2$ we obtain,

$$A_n^i N_{n+} e^{-ik_{xn}L/2} + A_n^0 N_{n-} e^{ik_{xn}L/2} = \sum_{m=-\infty}^{\infty} [a_m N'_{m+} e^{-iq_m L/2} + b_m N'_{m-} e^{iq_m L/2}] J_{n-m} \left(\frac{V_1}{\hbar\omega} \right) \quad (\text{A1})$$

$$\begin{aligned} & A_n^i N_{n+} S_+(E_n) e^{-ik_{xn}L/2} + A_n^0 N_{n-} S_-(E_n) e^{ik_{xn}L/2} \\ &= \sum_{m=-\infty}^{\infty} [a_m N'_{m+} S'_+(E_m) e^{-iq_m L/2} + b_m N'_{m-} S'_-(E_m) e^{iq_m L/2}] J_{n-m} \left(\frac{V_1}{\hbar\omega} \right) \end{aligned} \quad (\text{A2})$$

Similarly, boundary conditions at $x = L/2$ yields,

$$\begin{aligned} & B_n^i N_{n-} e^{-ik_{xn}L/2} + B_n^0 N_{n+} e^{ik_{xn}L/2} \\ &= \sum_{m=-\infty}^{\infty} [a_m N'_{m+} e^{iq_m L/2} + b_m N'_{m-} e^{-iq_m L/2}] J_{n-m} \left(\frac{V_1}{\hbar\omega} \right) \end{aligned} \quad (\text{A3})$$

$$\begin{aligned} & B_n^i N_{n-} S_-(E_n) e^{-ik_{xn}L/2} + B_n^0 N_{n+} S'_+(E_n) e^{ik_{xn}L/2} \\ &= \sum_{m=-\infty}^{\infty} [a_m N'_{m+} S'_+(E_m) e^{iq_m L/2} + b_m N'_{m-} S'_-(E_m) e^{-iq_m L/2}] J_{n-m} \left(\frac{V_1}{\hbar\omega} \right) \end{aligned} \quad (\text{A4})$$

Now, from above equations,

$$\begin{aligned} & A_n^i [S_-(E_n) - S_+(E_n)] e^{-ik_{xn}L/2} \\ &= \frac{1}{N_{n+}} \sum_{m=-\infty}^{\infty} [a_m N_{m+} (S_-(E_n) - S'_+(E_m)) e^{-iq_m L/2} + b_m N_{m-} (S_-(E_n) - S'_-(E_m)) e^{iq_m L/2}] J_{n-m} \left(\frac{V_1}{\hbar\omega} \right) \end{aligned} \quad (\text{A5})$$

$$\begin{aligned}
& B_n^i [S_-(E_n) - S_+(E_n)] e^{-ik_{xn}L/2} \\
&= \frac{1}{N_{n-}} \sum_{m=-\infty}^{\infty} [a_m N_{m+} (S'_+(E_m) - S_+(E_n)) e^{iq_m L/2} + b_m N_{m-} (S'_-(E_m) - S_+(E_n)) e^{-iq_m L/2}] J_{n-m} \left(\frac{V_1}{\hbar\omega} \right) \quad (\text{A6})
\end{aligned}$$

Now we define the matrices as -

$$(M_{sa}^{\pm})_{nm} = N'_{m+} \left[\left(\frac{1}{N_{n+}} \right) (S'_+(E_m) - S_-(E_n)) e^{i(k_{xn} - q_m)L/2} \pm \left(\frac{1}{N_{n-}} \right) (S_+ E_n - S'_+(E_m)) e^{i(k_{xn} + q_m)L/2} \right] J_{n-m} \left(\frac{V_1}{\hbar\omega} \right) \quad (\text{A7})$$

$$(M_{sb}^{\pm})_{nm} = N'_{m-} \left[\left(\frac{1}{N_{n+}} \right) (S'_-(E_m) - S_-(E_n)) e^{i(k_{xn} + q_m)L/2} \pm \left(\frac{1}{N_{n-}} \right) (S_+ E_n - S'_-(E_m)) e^{i(k_{xn} - q_m)L/2} \right] J_{n-m} \left(\frac{V_1}{\hbar\omega} \right) \quad (\text{A8})$$

$$(M_{cA}^1)_{nm} = \frac{N'_{m+}}{N_{n-}} e^{-i(q_m + k_{xn})L/2} J_{n-m} \left(\frac{V_1}{\hbar\omega} \right) \quad (\text{A9})$$

$$(M_{cA}^2)_{nm} = \frac{N'_{m-}}{N_{n-}} e^{i(q_m - k_{xn})L/2} J_{n-m} \left(\frac{V_1}{\hbar\omega} \right) \quad (\text{A10})$$

$$(M_{cB}^1)_{nm} = \frac{N'_{m+}}{N_{n+}} e^{i(q_m - k_{xn})L/2} J_{n-m} \left(\frac{V_1}{\hbar\omega} \right) \quad (\text{A11})$$

$$(M_{cB}^2)_{nm} = \frac{N'_{m-}}{N_{n+}} e^{-i(q_m + k_{xn})L/2} J_{n-m} \left(\frac{V_1}{\hbar\omega} \right) \quad (\text{A12})$$

$$(M_i)_{nm} = \frac{N_{n+}}{N_{n-}} e^{-ik_{xn}L} \delta_{n,m} \quad (\text{A13})$$

$$(M_r)_{nm} = (S_+(E_n) - S_-(E_n)) \delta_{n,m} \quad (\text{A14})$$

Appendix B: Scattering matrix

In this appendix we show the derivation for the S- matrix based on the boundary condition. The scattering matrix is defined as,

$$\begin{pmatrix} A^o \\ B^o \end{pmatrix} = \begin{pmatrix} M_{AA} & M_{AB} \\ M_{BA} & M_{BB} \end{pmatrix} \begin{pmatrix} A^i \\ B^i \end{pmatrix} = S \begin{pmatrix} A^i \\ B^i \end{pmatrix} \quad (\text{B1})$$

where, A^i and B^i represent the amplitudes of the incident wave and A^o and B^o represent the amplitudes of the outgoing signal and it can be shown that,

$$M_{AA} = M_{cA}^1 a_A + M_{cA}^2 b_A - M_i \quad (\text{B2})$$

$$M_{BA} = M_{cB}^1 a_A + M_{cB}^2 b_A \quad (\text{B3})$$

with,

$$a_A = [(M_{sb}^+)^{-1} M_{sa}^+ - (M_{sb}^-)^{-1} - M_{sa}^-]^{-1} [(M_{sb}^+)^{-1} - (M_{sb}^-)^{-1}] M_r \quad (\text{B4})$$

$$b_A = [(M_{sa}^+)^{-1} M_{sb}^+ - (M_{sa}^-)^{-1} - M_{sb}^-]^{-1} [(M_{sa}^+)^{-1} - (M_{sa}^-)^{-1}] M_r \quad (\text{B5})$$

Appendix C: Scattering Matrix

The scattering matrix is defined as,

$$\begin{pmatrix} A^o \\ B^o \end{pmatrix} = \begin{pmatrix} M_{AA} & M_{AB} \\ M_{BA} & M_{BB} \end{pmatrix} \begin{pmatrix} A^i \\ B^i \end{pmatrix} = S \begin{pmatrix} A^i \\ B^i \end{pmatrix} \quad (\text{C1})$$

Where, A^i and B^i represent the amplitudes of the incident wave and A^o and B^o represent the amplitudes of the outgoing signal and it can be shown that,

$$M_{AA} = M_{cA}^1 a_A + M_{cA}^2 b_A - M_i \quad (C2)$$

$$M_{BA} = M_{cB}^1 a_A + M_{cB}^2 b_A \quad (C3)$$

$$(C4)$$

With,

$$a_A = [(M_{sb}^+)^{-1} M_{sa}^+ - (M_{sb}^-)^{-1} - M_{sa}^-]^{-1} [(M_{sb}^+)^{-1} - (M_{sb}^-)^{-1}] M_r \quad (C5)$$

$$b_A = [(M_{sa}^+)^{-1} M_{sb}^+ - (M_{sa}^-)^{-1} - M_{sb}^-]^{-1} [(M_{sa}^+)^{-1} - (M_{sa}^-)^{-1}] M_r \quad (C6)$$

Appendix D: Quasi-bound Energies

In this section, we derive the energy of the quasi-bound state. These energies correspond to imaginary (real) wave-vectors outside (inside) the potential well resulting in the quasi-bound states to decay exponentially (propagate without decay) outside (inside) the potential well along the $\pm x$ -direction. Note that the electrons propagate freely along the y, z -directions. To investigate the quasi-bound states, we consider the wave function as given in Eq. (6) with $n = m = V_1 = 0$ as follows:

$$\psi_n = e^{-iEt/\hbar + ik_y y + ik_z z} \begin{cases} rN_- \begin{pmatrix} 1 \\ S_-(E) \end{pmatrix} e^{-ik_x x}, & x < -L/2 \\ [aN'_+ \begin{pmatrix} 1 \\ S'_+(E) \end{pmatrix} e^{iqx} + bN'_- \begin{pmatrix} 1 \\ S'_-(E) \end{pmatrix} e^{-iqx}], & -L/2 \leq x \leq L/2 \\ tN_+ \begin{pmatrix} 1 \\ S_+(E) \end{pmatrix} e^{ik_x x}, & x > L/2 \end{cases} \quad (D1)$$

Now, matching the boundary condition at $x = -L/2$ we get,

$$\begin{aligned} rN_- e^{ik_x L/2} - aN'_+ e^{-iqL/2} - bN'_- e^{iqL/2} &= 0 \\ rN_- S_-(E) e^{ik_x L/2} - aN'_+ S'_+(E) e^{-iqL/2} - bN'_- S'_-(E) e^{iqL/2} &= 0 \end{aligned}$$

Also, boundary condition at $x = +L/2$ gives -

$$\begin{aligned} tN_+ e^{-ik_x L/2} - aN'_+ e^{iqL/2} - bN'_- e^{-iqL/2} &= 0 \\ tN_+ S_+(E) e^{-ik_x L/2} - aN'_+ S'_+(E) e^{iqL/2} - bN'_- S'_-(E) e^{-iqL/2} &= 0 \end{aligned}$$

Secular determinant can be obtained by collecting the coefficients of $r, t, a,$ and b

$$\begin{vmatrix} N_- e^{ik_x L/2} & -N'_+ e^{-iqL/2} & -N'_- e^{iqL/2} & 0 \\ N_- S_-(E) e^{ik_x L/2} & -N'_+ S'_+(E) e^{-iqL/2} & -N'_- S'_-(E) e^{iqL/2} & 0 \\ 0 & -N'_+ e^{iqL/2} & -N'_- e^{-iqL/2} & N_+ e^{-ik_x L/2} \\ 0 & -N'_+ S'_+(E) e^{iqL/2} & -N'_- S'_-(E) e^{-iqL/2} & N_+ S_+(E) e^{-ik_x L/2} \end{vmatrix} = 0$$

This further yields the following determinant while the basis column matrix is given by $(N_- e^{ik_x L/2}, N'_+ e^{-iqL/2}, N'_- e^{iqL/2}, N_+ e^{-ik_x L/2})^T$ as follows

$$\begin{vmatrix} 1 & -1 & -1 & 0 \\ S_-(E) & -S'_+(E) & -S'_-(E) & 0 \\ 0 & -e^{iqL} & -e^{-iqL} & 1 \\ 0 & -S'_+(E) e^{iqL} & -S'_-(E) e^{-iqL} & S_+(E) \end{vmatrix} = 0$$

Solving the secular determinant and taking only the real part we arrive at - $q_n = \frac{(2n+1)\pi}{2L}$, $n \in \mathbb{Z}$
 From this, we can get the energy of quasi-bound states:

$$E_b = \left[V_0 \pm \hbar \sqrt{(2n+1)^2 \frac{\pi^2 t^2}{4L^2} + t^2 k_y^2 + s^2 t_z^2 k_z^2 \sin^2 k_0} \right] + \hbar k_z \tilde{t}$$

In our calculations, we consider $\hbar = 1$ for simplicity.

-
- [1] A. A. Burkov, *J. Phys. Condens. Matter* **27**, 113201 (2015).
- [2] B. Yan and C. Felser, *Annu. Rev. Condens. Matter Phys.* **8**, 337 (2017).
- [3] N. P. Armitage, E. J. Mele, and A. Vishwanath, *Rev. Mod. Phys.* **90**, 015001 (2018).
- [4] E. V. Gorbar, V. A. Miransky, I. A. Shovkovy, P. O. Sukhachov, *Low Temperature Physics* **44**, 487 (2018).
- [5] H. Weng, C. Fang, Z. Fang, B. A. Bernevig, and X. Dai, *Phys. Rev. X* **5**, 011029 (2015).
- [6] Huang, S., Xu, S., Belopolski, I. et al., *Nat. Commun.* **6**, 7373 (2015).
- [7] B. Yan and C. Felser, *Annu. Rev. Condens. Matter Phys.* **8** 337 (2017).
- [8] M. Z. Hasan, S.-Y. Xu, I. Belopolski, and C.-M. Huang, *Annu. Rev. Condens. Matter Phys.* **8**, 289 (2017).
- [9] G. Xu, H. Wend, Z. Wang, X. Dai, and Z. Fang, *Phys. Rev. Lett.* **107**, 186806 (2011).
- [10] C. Fang, M. J. Gilbert, X. Dai, and B. A. Bernevig, *Phys. Rev. Lett.* **108**, 266802 (2012).
- [11] A. A. Soluyanov, D. Gresch, Z. Wang, Q. Wu, M. Troyer, X. Dai, and B. A. Bernevig, *Nature* **527**, 495-498 (2015).
- [12] G. Autes, D. Gresch, M. Troyer, A. A. Soluyanov, and O. V. Yazyev, *Phys. Rev. Lett.* **117**, 066402 (2016).
- [13] M.-Y. Yao, N. Xu, Q. S. Wu, G. Autes, N. Kumar, V. N. Strocov, N. C. Plumb, M. Radovic, O. V. Yazyev, C. Felser, J. Mesot, and M. Shi, *Phys. Rev. Lett.* **122**, 176402 (2019).
- [14] H. Nielsen and M. Ninomiya, *Phys. Lett. B* **130**, 389 (1983).
- [15] T. Nag, S. Nandy, *J. Phys.: Condens. Matter* **33**, 075504 (2021).
- [16] B. Sadhukhan, T. Nag, *Phys. Rev. B* **107**, L081110 (2023).
- [17] A. Menon and B. Basu, *J. Phys.: Condens. Matter* **33** 045602 (2021).
- [18] F. Xiong, C. Honerkamp, D. M. Kennes, T. Nag, *Phys. Rev. B* **106**, 045424 (2022).
- [19] S. K. Das, T. Nag, S. Nandy, *Phys. Rev. B* **104**, 115420 (2021).
- [20] B. Sadhukhan, T. Nag, *Phys. Rev. B* **103**, 144308 (2021).
- [21] B. Sadhukhan, T. Nag, *Phys. Rev. B* **104**, 245122 (2021).
- [22] T. Nag, D. M. Kennes, *Phys. Rev. B* **105**, 214307 (2022).
- [23] T. E. O. Brien, M. Diez, C. W. J. Beenakker, *Phys. Rev. Lett.* **116**, 236401 (2016).
- [24] Zyuzin, A.A., Tiwari, R.P., *JETP Lett.* **103**, 717-722 (2016).
- [25] Maximilian Trescher, Björn Sbierski, Piet W. Brouwer, and Emil J. Bergholtz, *Phys. Rev. B* **91**, 115135 (2015).
- [26] T. Oka and H. Aoki, *Physical Review B* **79**, 081406(R) (2009).
- [27] T. Kitagawa, E. Berg, M. Rudner, and E. Demler, *Phys. Rev. B* **82**, 235114 (2010).
- [28] M. S. Rudner, N. H. Lindner, E. Berg, and M. Levin, *Phys. Rev. X* **3**, 031005 (2013).
- [29] F. Nathan and M. S. Rudner, *New Journal of Physics* **17**, 125014 (2015).
- [30] P. Titum, E. Berg, M. S. Rudner, G. Refael, and N. H. Lindner, *Phys. Rev. X* **6**, 021013 (2016).
- [31] T. Nag, S. Roy, A. Dutta, D. Sen, *Phys. Rev. B* **89**, 165425 (2014).
- [32] T. Nag, R-J Slager, T. Higuchi, T. Oka, *Phys. Rev. B* **100**, 134301 (2019).
- [33] L. Tamang, T. Nag, T. Biswas, *Phys. Rev. B* **104**, 174308 (2021).
- [34] T. Nag, A. Rajak, *Phys. Rev. B* **104**, 134307 (2021).
- [35] A. Kundu, A. Rajak, T. Nag, *Phys. Rev. B* **104**, 075161 (2021).
- [36] H. C. Po, L. Fidkowski, T. Morimoto, A. C. Potter, and A. Vishwanath, *Phys. Rev. X* **6**, 041070 (2016).
- [37] S. Kar and B. Basu, *Phys. Rev. B* **98**, 245119 (2018).
- [38] J. H. Shirley, *Phys. Rev.* **138**, B979 (1965).
- [39] M. Holthaus and D. Hone, *Phys. Rev. B* **47**, 6499 (1993).
- [40] T. Fromherz, *Phys. Rev. B* **56**, 4772 (1997).
- [41] A. Menon, D. Chowdhury, and B. Basu, *Phys. Rev. B* **98**, 205109 (2018).
- [42] T. Nag, A. Menon, and B. Basu, *Phys. Rev. B* **102**, 014307 (2020).
- [43] Zhang, B., Maeshima, N., and Hino, Ki., *Sci. Rep.* **11**, 2952 (2021).
- [44] Kumar, U., Banerjee, S., and Lin, S.Z., *Nat. Commun. Phys.* **5**, 157 (2022).
- [45] U. Fano, *Nuovo Cimento* **12**, 154 (1935).
- [46] A. E. Miroshnichenko, S. Flach, and Y. S. Kivshar, *Rev. Mod. Phys.* **82**, 2257 (2010).
- [47] B. Lukyanchuk, N. I. Zheludev, S. A. Maier, N. J. Halas, P. Nordlander, H. Giessen, and C. T. Chong, *Nat. Mater.* **9**, 707 (2010).
- [48] E. Tekman and P. F. Bagwell, *Phys. Rev. B* **48**, 2553 (1993).
- [49] H. G. Luo, T. Xiang, X. Q. Wang, Z. B. Su, and L. Yu, *Phys. Rev. Lett.* **92**, 256602 (2004).
- [50] A. C. Johnson, C. M. Marcus, M. P. Hanson, and A. C. Gossard, *Phys. Rev. Lett.* **93**, 106803 (2004).
- [51] B. R. Bulka and P. Stefanski, *Phys. Rev. Lett.* **86**, 5128 (2001).
- [52] M. E. Torio, K. Hallberg, S. Flach, A. E. Miroshnichenko, and M. Titov, *Eur. Phys. J. B* **37**, 399 (2004).
- [53] C. S. Chu and R. S. Sorbello, *Phys. Rev. B* **40**, 5941 (1989).
- [54] R. Zhu, *J. Phys.: Condens. Matter* **25**, 036001 (2013).
- [55] T. B. Boykin, B. Pezeshki, and J. S. Harris, *Phys. Rev. B* **46**, 12769 (1992).

- [56] W. Porod, Z. Shao, and C. S. Lent, *Appl. Phys. Lett.* **61**, 1350 (1992).
- [57] J. L. Cardoso and P. Pereyra, *Europhys. Lett.* **83**, 38001 (2008).
- [58] K. Kobayashi, H. Aikawa, A. Sano, S. Katsumoto, and Y. Iye, *Phys. Rev. B* **70**, 035319 (2004).
- [59] R. Zhu and M. Liu, *Eur. Phys. J. B* **89**, 2 (2016).
- [60] R. Zhu, J.-H. Dai, and Y. Guo, *J. Appl. Phys.* **117**, 164306 (2015).
- [61] R. Zhu, C. Cai, *J. Appl. Phys.* **122**, 124302 (2017).
- [62] S. Bera and I. Mandal, *J. Phys.: Condens. Matter* **33**, 295502 (2021).
- [63] S. Bera, S. Sekh, I. Mandal, *Ann. Phys. (Berlin)* **535**, 2200460 (2023).
- [64] A. Gregefalk, A. Black-Schaffer, T. Nag, [arXiv:2306.08759](https://arxiv.org/abs/2306.08759) (2023).
- [65] W. Li and L. E. Reichl, *Phys. Rev. B* **60**, 15732 (1999).
- [66] Y. M. Blanter and M. Büttiker, *Physics reports* **336**, 1 (2000).
- [67] U. Fano, *Phys. Rev.* **124** 1866 (1961).
- [68] M. Milicevic, G. Montambaux, T. Ozawa, O. Jamadi, B. Real, I. Sagnes, A. Lemaitre, L. Le Gratiet, A. Harouri, J. Bloch, and A. Amo, *Phys. Rev. X* **9**, 031010 (2019).
- [69] A. Cortijo, D. Kharzeev, K. Landsteiner, M. A. H. Vozmediano, *Phys. Rev. B* **94**, 241405(R) (2016).
- [70] D. I. Pikulin, Anffany Chen, and M. Franz, *Phys. Rev. X* **6**, 041021 (2016).
- [71] A. G. Grushin, J. W. F. Venderbos, A. Vishwanath, and R. Ilan, *Phys. Rev. X* **6**, 041046 (2016).
- [72] R. W. Bomantara and J. Gong, *Phys. Rev. B* **94**, 235447 (2016).
- [73] M. O. Goerbig, J.-N. Fuchs, G. Montambaux, and F. Piechon, *Phys. Rev. B* **78**, 45415 (2008).
- [74] H-Y Lu, A. S. Cuamba, S-Y Lin, L. Hao, R. Wang, H. Li, Y. Zhao, and C. S. Ting, *Phys. Rev. B* **94**, 195423 (2016).
- [75] A. D. Zabolotskiy and Yu. E. Lozovik, *Phys. Rev. B* **94**, 165403 (2016).
- [76] R. G. Polozkov, N. Y. Senkevich, S. Morina, P. Kuzhir, M. E. Portnoi, and I. A. Shelykh, *Phys. Rev. B* **100**, 235401 (2019).
- [77] J-P. Lang, H. Hanafi, J. Imbrock, and C. Denz, *Phys. Rev. A* **107**, 023509 (2023).
- [78] B. W. Shore, *Rev. Mod. Phys.* **39**, 439 (1967).
- [79] F. Smith, *Phys. Rev.* **118**, 349 (1960).